

See discussions, stats, and author profiles for this publication at: <https://www.researchgate.net/publication/6931782>

# Corrosion Inhibitors: Design, Performance, and Computer Simulations

ARTICLE *in* THE JOURNAL OF PHYSICAL CHEMISTRY B · JANUARY 2006

Impact Factor: 3.3 · DOI: 10.1021/jp0522765 · Source: PubMed

---

CITATIONS

33

---

READS

163

5 AUTHORS, INCLUDING:



**Monica Galicia**

Universidad Autónoma de Ciudad Juárez

17 PUBLICATIONS 182 CITATIONS

SEE PROFILE



**Hiram Isaac Beltran**

Metropolitan Autonomous University

78 PUBLICATIONS 833 CITATIONS

SEE PROFILE

# Corrosion Inhibitors: Design, Performance, and Computer Simulations

Yurko Duda,<sup>\*,†,‡</sup> Roberto Govea-Rueda,<sup>†</sup> Mónica Galicia,<sup>†</sup> Hiram I. Beltrán,<sup>\*,†</sup> and Luis S. Zamudio-Rivera<sup>\*,†</sup>

*Programa de Ingeniería Molecular, Instituto Mexicano del Petróleo, Eje Central L. Cárdenas 152, 07730, México, D. F., and Institute for Condensed Matter Physics, NAS of Ukraine, 79011, Lviv, Ukraine*

*Received: May 2, 2005; In Final Form: August 16, 2005*

The development of a methodology to predict the performance of a corrosion inhibitor (CI) using specific types of modeled and experimental surfaces and their subsequent estimation is presented. For previously reported imidazoline CIs, the theoretical partition coefficients and molecular volumes were calculated, providing a guide for molecular engineering of new imidazolines. The new CIs, *N*-[2-(2-alkyl-4,5-dihydroimidazol-1-yl)ethyl]alkylamides and *N*-[2-(2-alkyloylaminoethylamino)ethyl]alkylamides, were designed, prepared, and their theoretical partition coefficients and molecular volumes calculated. These indexes were correlated between tested and prototype CIs to select the best ones for the corrosion inhibition tests. The inhibition efficiencies were measured through potentiodynamic polarization curves (PPC), linear polarization resistance (LPR), and weight loss measurements (WLM) for SAE-1010 and SAE-1018 steels. The leading molecules were 1-(2-decylaminoethyl)-2-decylimidazoline and 1-(2-dodecylaminoethyl)-2-dodecylimidazoline with WLM efficiencies (steel 1010), of 62.8 and 78.9%, respectively. The efficiencies for the PPC/LPR tests (steel 1018) were 97 and 94%. To understand the mechanism of action of CIs, a simple model is suggested for the growth of self-assembled monolayers of CIs on a crystalline substrate. This model takes into account the amphiphilic nature of the inhibitor molecule on the adsorption process. Despite the simplicity of the model, the Monte Carlo simulations reproduce qualitatively many of the experimentally observed features involved in the formation of monolayers and provide a tentative explanation for the mechanism of corrosion inhibition.

## Introduction

Corrosion represents a major industrial setback, which causes the detriment of materials and considerable economic losses.<sup>1</sup> The corrosion phenomenon is particularly important for the alkaline–acid sections of the oil industry, namely, the atmospheric distillation plants, pipelines, vacuum vessels, hydrosulfuration plants, and catalytic reactors.<sup>2,3</sup> To overcome this unavoidable problem, the streamline is the use of corrosion inhibitors (CI),<sup>4,5</sup> which can be defined as, “any chemical substance or substances, which when added to an aggressive system, in small amounts, significantly diminish the corrosion rate”. The availability of CIs is wide, and the development of new prototypes with enhanced efficiencies, which satisfy environmental requirements, and understanding of the corrosion/inhibition mechanism are research goals worldwide.<sup>6,7</sup> A vast number of studies have led to the design of imidazoline (IM) type molecules due to their improved efficiency and low production cost.<sup>4,8–14</sup> Unfortunately, IMs depict water-dependent imidazoline–amide equilibrium, giving rise to different conclusions regarding the inhibition performance. Jovanicevic and co-workers<sup>14</sup> have found that alkyl-IMs are less efficient CIs than their alkylamidic precursors. Recently, alkyl-IMs were found to be more efficient CIs than their amidic precursors.<sup>8</sup> These discrepancies should be understood.

Along this line, the development of molecular simulation and quantum model approximation have been successfully applied

to solve this problem.<sup>15–17</sup> Theoretical methods to model monolayers include integral equation<sup>18–20</sup> density functional theory<sup>21</sup> and mean-field theories,<sup>22</sup> as well as thermodynamic formalisms.<sup>23</sup> While the application of detailed molecular potentials and statistical mechanical methods to answer many application problems is of great interest, the development of simple analytical and numerical models remains alive and continues to emerge in the literature.<sup>15,24,25</sup> The development of a microscopic model is a common practice in the study and understanding of physicochemical systems. Such a microscopic model, which is often roughly defined, takes into account a few of the essential characteristics of the system under study (e.g., molecular flexibility, solubility, diffusion, etc.) instead of the detailed chemical structure and more robust physicochemical data. This provides a useful way to elucidate the important factors affecting a particular phenomenon, such as corrosion.<sup>15,22–26</sup>

A systematic study of two full series of imidazolinic and amidic precursors as new prototypes of CIs is herein developed. These compounds were selected, synthesized, characterized, and evaluated based on theoretical calculations due to their molecular analogy with previously tested CI imidazolines. Moreover, the mechanism for the formation of CI monolayers suggests the essential features such as (a) strong bonding of the headgroup; (b) self-organization of the tails to form a coherent solvophobic film, which serves as a barrier for the migration and interaction of general pollutants with the metallic surface; and (c) lyophilic/lyophobic balance of CI molecules.

## Experimental Section

**Materials and Equipment.** NMR spectra were obtained in a Varian Mercury 200-BB spectrometer; chemical shifts are given in ppm, coupling constants in hertz; in all cases, the used

\* To whom correspondence should be addressed. E-mail: yduda@lycos.com(Y.D.); hbeltran@imp.mx(H.I.B.); lzamudio@imp.mx(L.S.Z.-R.). Telephone: (52)-55-9175-8269. Fax: (52)-55-9175-6239.

<sup>†</sup> Instituto Mexicano del Petróleo.

<sup>‡</sup> NAS of Ukraine.

solvent was deuterated chloroform and as internal reference tetramethylsilane. IR spectra were obtained in a Bruker Tensor 27 spectrometer. The IR spectra were measured as KBr pellets or as neat liquids through the ATR technique; the direct detection technique was horizontal automatic target recognition. Melting points were measured in open capillary tubes using Electrothermal 9300 equipment and are uncorrected. All reagents were purchased from Aldrich Co. and used as received unless otherwise stated.

**Synthetic Route.** Detailed experimental procedures for the preparation of prototype molecules are given as Supporting Information.

**Electrochemical Tests. Experimental Device.** Electrochemical tests to determine corrosion inhibition efficiencies were performed on an Autolab potentiostat/galvanostat model PG-STAT30 with the Autolab interface and the GPES software.<sup>27</sup> Each experiment was determined with a conventional three-electrode cell in hydrodynamic conditions. The reference was a saturated calomel electrode, and the counter electrode was a platinum screen. A salt bridge, with saturated KCl solution, connected the cell with the reference electrode.

**Preparation of Samples.** The working electrode was an 8-mm-diameter SAE 1018 steel cylinder with a typical composition of 0.14–0.20% C, 0.60–0.90% Mn, maximum 0.03% P, maximum 0.035% S, and the remaining Fe. The electrode was embedded in a Teflon base, in such a way that the transversal area of 0.5 cm<sup>2</sup> was the only section directly exposed to the aggressive media. This was followed by treatment with a polyester resin and a styrene mixture to avoid filtration of the solution. The initial electrode surface was prepared by polishing with 400-grit silicon carbide sand paper and distilled water, followed by 600-grit sand paper and distilled water until a homogeneous surface was obtained. Finally, the electrode was rinsed with acetone and used immediately. This procedure was repeated throughout the measurements, which were performed at room temperature.

**Electrolytic Media.** The electrolytes were hydrochloric acid and sour brine solutions.<sup>28</sup> A 1 N HCl solution was prepared according to the ASTM standard,<sup>29</sup> from 169.49 mL of 36.5% (w/w) hydrochloric acid and distilled water. The H<sub>2</sub>S brine was prepared in distilled water (previously degassed with nitrogen) from 60 000 ppm (71.2%) NaCl, 6613 ppm (7.8%) CaCl<sub>2</sub>·2H<sub>2</sub>O, 10 680 ppm (12.7%) MgCl<sub>2</sub>·2H<sub>2</sub>O, and 3493 ppm (4.2%) Na<sub>2</sub>SO<sub>4</sub>, utilizing a gas stream of H<sub>2</sub>S at a rate of 0.6 L·min<sup>-1</sup>, until a pH of 4 was achieved. Due to the aggressiveness of H<sub>2</sub>S to human health, preparation of the sour brine was performed in an aerated hood; after every set of electrochemical tests, the solution was placed into an industrial freezer to avoid H<sub>2</sub>S losses. Fresh sour brine was prepared every day for the testing period.

**Inhibitor Solutions.** A 10000 ppm solution was prepared by dissolving 0.100 g of each specific CI in 10 mL of 2-propanol, using a 10-mL volumetric flask, and the solution was stirred for 10 min. 2-Propanol dilutions from the 10 000 to 1000 and 500 ppm solutions were carried out. Solutions of 10, 25, 50, and 100 ppm were prepared for each CI following the latter dilution procedure but using the respective acidic media. As an example, preparation of the 10 ppm solution is described. An aliquot of 2 mL was taken from the 500-mL solution, diluted with 1 N HCl using a volumetric 100-mL flask, and stirred during 10 min.

**Corroded Surface Emulation for HCl and H<sub>2</sub>S Environments.** The corrosion process was emulated by applying a potential and monitored with the GPES software. Polarization curves were recorded from -250 to +250 mV versus the OCP with a scan rate of 3 mV·s<sup>-1</sup> starting 5 min after immersion of

the working electrode into the solution. These experimental conditions were employed for all reported data. The anodic ( $\beta_a$ ) and cathodic ( $\beta_c$ ) Tafel constants, the corrosion potential ( $E_{\text{corr}}$ ), and the corrosion current density ( $j_{\text{corr}}$ , from the Stern–Geary equation) were determined following the ASTM standard.<sup>30–34</sup> and using Autolab GPES analysis technique. The polarization resistance ( $R_p$ ) was evaluated from the same polarization curves setting a small overpotential of  $\pm 15$  mV versus OCP on the working electrode and measuring the resulting current under steady-state conditions. All plots and calculated parameters are means of five independent experiments. The average standard deviation is reported as well.

**Weight Loss Measurements.** A dynamic evaluator model C5-EDP-020-D with a NACE TM-01-7-2001<sup>35</sup> solution was used for weight loss measurements (WLM). The selected coupons were made from SAE-1010 carbon steel having 0.07–0.08% C, 0.08–0.09% P, and 0.034–0.037% Mn and the following dimensions, 2.54 cm  $\times$  1.27 cm  $\times$  0.025 cm. The specimens were not polished, and the aggressive medium was a 1 N HCl solution. Each run was made at room temperature.

**Solution Preparations.** The 1 N HCl and 10, 25, 50, and 100 ppm CI solutions were prepared as described in the electrochemical tests. An inhibited acid solution was prepared from 100 mL of 36.5% (w/w) HCl, 2.0 g of antimony(VI) trioxide, and 5.0 g of tin(II) dichloride dihydrate, and the mixture was stirred for 10 min.

**Weight Loss Evaluation.** Each specimen was rinsed with chloroform and then hexanes; direct contact with the skin was avoided throughout the experiments. All specimens were weighed in pairs, placed into 250-mL glassware, and the aggressive 1 N HCl solution was added and followed by the corresponding solution of CI at concentrations between 10, 25, 50, and 100 ppm. The gravimetric test was allowed to stand for 5 h at 70 °C with vigorous stirring. The procedure was standardized, and the data show that all corrosion rates are very similar to those for the potentiodynamic polarization curve/linear polarization resistance (PPC/LPR) tests. All tests were repeated twice for each concentration and reference. At the end of the test, the specimens were rinsed with chloroform, acetone, and water and washed with the inhibited acid solution, with a 5% (w/w) potassium bicarbonate solution, and finally with water. After that, each specimen was iron-brushed and washed with water, oven-dried at 60 °C, weighed again, and this value reported as the final mass.<sup>8,36,37</sup>

The inhibitor efficiency (IE, %) was calculated from the gravimetric and potentiodynamic data.

## Results and Discussion

**Semiempirical Determination of Partition Coefficient and Molecular Volume.** By a systematical analysis of the CI molecular components, the IM head moiety is known to have an efficient interaction with metallic surfaces. Hence, this fragment was fixed for the design.<sup>4,8,14,16,17</sup> Semiempirical calculations with the PM3<sup>38,39</sup> chemical model were done to obtain the partition coefficient ( $\log P$ ) and the molecular volume ( $V_{\text{mol}}$ ) indexes from published 1-(2-hydroxyethyl)-2-alkylimidazolines **1a–g** (Figure 1a).<sup>8</sup> These two indexes were chosen because  $\log P$  is related to the polarization/solubility and protection of the surface.<sup>40</sup> The molecular volume,  $V_{\text{mol}}$ , is related to the covered surface by a molecule itself.<sup>41</sup> This report<sup>8</sup> had shown that **1f** and **1g** were the most efficient CIs for acidic media.<sup>8</sup> The results from this analysis are summarized in Table 1.

Compounds of type **1** have shown to be good CIs, and for tractable reasons, the new prototypes should possess similar physicochemical values to ensure at least equal inhibition effi-

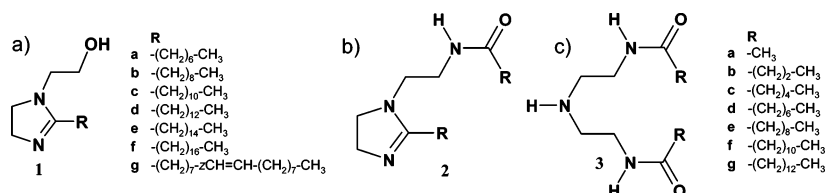


**Figure 1.** (a) 1-(2-Hydroxyethyl)-2-alkylimidazolines **1a–g** as model CI molecule, (b) *N*-[2-(2-alkyl-4,5-dihydroimidazol-1-yl)ethyl]alkylamides **2a–g**, and (c) *N*-[2-(2-alkylolaminoethylamino)ethyl]alkylamides **3a–g** as prototype CI molecules.

**TABLE 1: Theoretical Physicochemical Properties for 1a–g, 2a–g, and 3a–g, and Inhibition Efficiencies (IE) for 1a–g<sup>a</sup>**

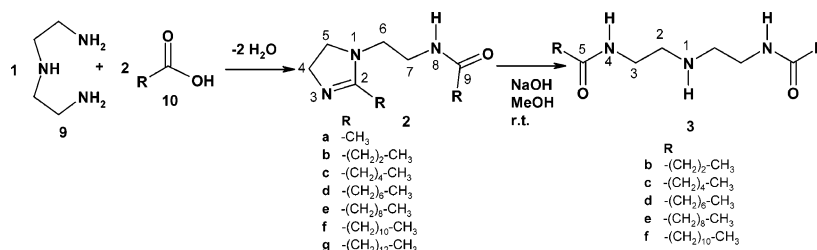
compound	log <i>P</i>	<i>V</i> <sub>mol</sub> (Å <sup>3</sup> )	IE, at 7.5 ppm <sup>a</sup> (%)
<b>1a<sup>a</sup></b>	2.32	786.98	31.7
<b>1b<sup>a</sup></b>	3.11	894.63	41.3
<b>1c<sup>a</sup></b>	3.90	1002.26	48.5
<b>1d<sup>a</sup></b>	4.69	1108.54	68.9
<b>1e<sup>a</sup></b>	5.49	1216.12	83.0
<b>1f<sup>a</sup></b>	6.28	1309.65	96.3
<b>1g<sup>a</sup></b>	6.02	1293.33	96.2
<b>2a</b>	−0.82	575.09	<i>c</i>
<b>2b</b>	1.23	753.36	<i>c</i>
<b>2c</b>	2.82	920.40	<i>c</i>
<b>2d</b>	4.40	1098.31	<i>c</i>
<b>2e</b>	5.59	1271.83	<i>c</i>
<b>2f</b>	7.57	1447.06	<i>c</i>
<b>2g</b>	9.16	1660.23	<i>c</i>
<b>3a</b>	−2.13	652.30	<i>c</i>
<b>3b</b>	−0.08	798.27	<i>c</i>
<b>3c</b>	1.50	1006.89	<i>c</i>
<b>3d</b>	3.09	1177.70	<i>c</i>
<b>3e</b>	4.67	1331.94	<i>c</i>
<b>3f</b>	6.26	1521.13	<i>c</i>
<b>3g</b>	7.84	1674.22	<i>c</i>

<sup>a</sup> Calculations performed at PM3 level of theory. <sup>b</sup> Taken from ref 8. <sup>c</sup> Data not already available.

ciencies. The new *N*-[2-(2-alkyl-4,5-dihydroimidazol-1-yl)ethyl]-alkylamides **2a–g** are proposed as prototype IM-CIs (Figure 1b). Hence, the log *P* and the *V*<sub>mol</sub> for **1** were theoretically determined and are summarized in Table 1. The *N*-[2-(2-alkylolaminoethylamino)ethyl]alkylamides **3a–g**, derived from **2a–g** (Figure 1c) could possess comparable corrosion inhibition efficiencies and should be tested as non IM-CIs as well (Table 1). A comparison between **2a–g** and **3a–g** CIs should fulfill the proper comparison regarding the energetic difference among imidazoline nitrogen atoms (sp<sup>2</sup> nature) and secondary amine nitrogen atoms (sp<sup>3</sup> nature) toward the surface-CI reaction. By analyzing the obtained theoretical indexes, and taking **1f** and **1g** as lead compounds, the most efficient CIs should be found among **2e**, **2f**, **3d**, **3e**, and **3f**.

**Synthesis and Characterization of Compounds 2b–g and 3b–f.** Based on molecular calculations, the best compounds were synthesized (Scheme 1) avoiding the preparation of **2a**, **3a**, and **3g**, because of their log *P* and *V*<sub>mol</sub> values (Table 1).

**SCHEME 1: Reaction between DETA (9) and Carboxylic Acids 10b–g To Obtain 2b–g and Hydrolysis Reaction of 2b–f To Give 3b–f<sup>a</sup>**



<sup>a</sup> Numbering used for NMR addnment.

The preparation of **2b–g** was performed by triple condensation reaction of diethylenetriamine **9** with the corresponding carboxylic acids **10b–g** in a 1:2 stoichiometric ratio, to yield the corresponding *N*-[2-(2-alkyl-4,5-dihydroimidazol-1-yl)ethyl]-alkylamides **2b–g**. Compounds **2b** and **2c** were distilled while **2d–g** were purified by the addition of 20 mL of acetone, vigorous stirring, and filtration of the pure solid. The yields of isolated products were between 59 and 94%. The amidic compounds, **3b–f**, were obtained from **2b–f** by hydrolysis in methanol, and sodium hydroxide at room temperature for 2 h (Scheme 1). The procedure provided pure **3b–f** in yields between 47 and 92%.

The <sup>1</sup>H, <sup>13</sup>C NMR, and IR data and assignment for **2b–g** and **3b–f** are given as Supporting Information.

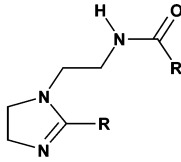
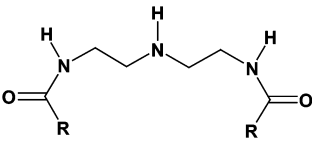
**Electrochemical and Weight Loss Evaluations of Inhibition Efficiencies.** Table 2 shows the corrosion inhibition efficiencies (%) in HCl media, obtained by the potentiodynamic polarization curves, and linear polarization resistance, at concentrations of 10, 25, 50, and 100 ppm for **2b–g** and **3b–f**. The corrosion inhibition efficiencies and rates were calculated for inhibitors **2d**, **2e**, **2f**, and **2g** at the same concentrations but in a brine containing H<sub>2</sub>S (Table 2) in order to evaluate the performance in different media. The latter inhibitors were chosen, as they provide, a priori, the best corrosion inhibition performance in HCl media. Analysis of the data indicates that for the **2** and **3** series, efficiency increases as the concentration increases when the 10 and 100 ppm samples in HCl and H<sub>2</sub>S environments were compared. In fact, type **2** molecules were more efficient at inhibiting the HCl than the H<sub>2</sub>S media.

The Mexican oil industry (PEMEX) sets as a standard the use of less than 25 ppm of corrosion inhibitor concentrations due to monetary implications.<sup>8–11</sup> According to this criterion and following the data in Table 2, the efficiency of type **2** compounds is a function of the hydrocarbon chain length and therefore of the partition coefficient and the molecular volume. Specifically, at 10 ppm, the most efficient compounds were **2e** and **2f** in both HCl and H<sub>2</sub>S environments, as successfully predicted with the PM3 approach.

Comparative analyses among compounds of types **2** and **3** at concentrations of 25 ppm or less show that the former are better corrosion inhibitors, indicating that the electronic pair of nitrogen atoms is responsible for stronger binding with the iron atoms



TABLE 2: Corrosion Inhibition Efficiencies (IE, %) by PPC/LPR and WLM for 2b–g and 3b–f in HCl and H<sub>2</sub>S<sup>a</sup>

	R				R	
	2b	-(CH <sub>2</sub> ) <sub>2</sub> -CH <sub>3</sub>	3b	-(CH <sub>2</sub> ) <sub>2</sub> -CH <sub>3</sub>		
	2c	-(CH <sub>2</sub> ) <sub>4</sub> -CH <sub>3</sub>	3c	-(CH <sub>2</sub> ) <sub>4</sub> -CH <sub>3</sub>		
	2d	-(CH <sub>2</sub> ) <sub>6</sub> -CH <sub>3</sub>	3d	-(CH <sub>2</sub> ) <sub>6</sub> -CH <sub>3</sub>		
	2e	-(CH <sub>2</sub> ) <sub>8</sub> -CH <sub>3</sub>	3e	-(CH <sub>2</sub> ) <sub>8</sub> -CH <sub>3</sub>		
	2f	-(CH <sub>2</sub> ) <sub>10</sub> -CH <sub>3</sub>	3f	-(CH <sub>2</sub> ) <sub>10</sub> -CH <sub>3</sub>		
	2g	-(CH <sub>2</sub> ) <sub>12</sub> -CH <sub>3</sub>				
Compound	Concentration (ppm)	(mmol·L <sup>-1</sup> )	Corrosion Rate (mpy) PPC	WLM	IE (%) PPC	WLM
2b MW=225.34	10	0.0444	277±8	---	21.9	---
	25	0.1109	114±4	---	67.9	---
	50	0.2219	100±5	---	71.7	---
	100	0.4438	102±4	---	71.0	---
2c MW=281.44	10	0.0355	96.7±2.5	---	72.7	---
	25	0.0888	81.3±1.7	---	77.1	---
	50	0.1777	89.8±2.2	---	74.7	---
	100	0.3553	54.8±1.7	---	84.6	---
2d MW=337.55	10	0.0296	57.9±0.6 / 8.5±0.4 <sup>a</sup>	138.5	83.7 / 81.8 <sup>a</sup>	32.2
	25	0.0741	22.3±0.7 / 7.6±0.2 <sup>a</sup>	82.9	93.7 / 83.1 <sup>a</sup>	59.4
	50	0.1481	21.2±0.8 / 7.4±0.5 <sup>a</sup>	103.3	94.0 / 81.4 <sup>a</sup>	49.5
	100	0.2963	5.6±0.12 / 9.4±0.4 <sup>a</sup>	134.3	98.4 / 72.7 <sup>a</sup>	34.3
2e MW=393.66	10	0.0254	35.1±0.7 / 6.9±0.1 <sup>a</sup>	93.5	90.1 / 84.6 <sup>a</sup>	54.2
	25	0.0635	42.1±0.7 / 7.6±0.6 <sup>a</sup>	75.9	88.2 / 71.9 <sup>a</sup>	62.8
	50	0.1270	26.7±1.0 / 7.9±0.8 <sup>a</sup>	78.3	92.5 / 91.3 <sup>a</sup>	61.7
	100	0.2540	10.7±0.7 / 8.6±0.8 <sup>a</sup>	134.2	97.0 / 80.8 <sup>a</sup>	34.3
2f MW=449.77	10	0.0222	19.1±1.1 / 5.5±0.4 <sup>a</sup>	51.9	94.6 / 87.8 <sup>a</sup>	74.6
	25	0.0556	27.1±1.1 / 5.0±0.3	43.1	92.4 / 88.9 <sup>a</sup>	78.9
	50	0.1112	32.0±1.2 / 5.3±0.3 <sup>a</sup>	51.9	91.0 / 88.1 <sup>a</sup>	74.6
	100	0.2223	18.2±1.4 / 5.5±0.9 <sup>a</sup>	68.5	94.9 / 87.8 <sup>a</sup>	66.5
2g MW=505.88	10	0.0198	58.1±2.0 / 9.5±0.4 <sup>a</sup>	71.8	83.6 / 79.0 <sup>a</sup>	64.9
	25	0.0494	42.1±1.8 / 9.1±0.5 <sup>a</sup>	63.9	88.2 / 80.0 <sup>a</sup>	68.7
	50	0.0988	26.7 ±1.6 / 8.4±0.5 <sup>a</sup>	34.3	92.5 / 81.0 <sup>a</sup>	83.2
	100	0.1977	10.7±1.0 / 5.6±0.4 <sup>a</sup>	94.0	97.0 / 88.0 <sup>a</sup>	54.0
3b	10	---	447±11	---	-25.9	---
	25	---	228±7	---	35.5	---
	50	---	185±8	---	47.8	---
	100	---	102±9	---	71.1	---
3c	10	---	407±10	---	-14.9	---
	25	---	287±8	---	19.0	---
	50	---	185±11	---	47.7	---
	100	---	80.9±4	---	77.2	---
3d	10	---	55.7±5	510.4	19.8	-149.8
	25	---	10.9±0.6	145.9	35.5	28.6
	50	---	23.64±0.6	90.3	50.9	55.8
	100	---	35.6±0.9	112.5	93.3	44.9
3e	10	---	265±10	243.6	25.3	19.2
	25	---	210±6	141.3	40.6	30.9
	50	---	114±4	119.0	67.6	41.8
	100	---	14.6±1.1	124.1	95.9	39.3
3f	10	---	307±9	139.4	13.4	31.8
	25	---	204±6	98.6	42.5	51.7
	50	---	64.9±4	76.9	81.7	62.4
	100	---	24.8±1.5	72.3	93.0	64.6
Reference	---	---	354.±9 / 44.8±1.5 <sup>a</sup>	204.4	---	---

of the surface. Thus, compounds with imidazolinic nitrogen atoms build more resistant films than compounds with secondary aminic nitrogen atoms.

In PEMEX, the applied field methodology to evaluate the performance of a corrosion inhibitor is WLM of steel specimens.<sup>35</sup> Therefore, gravimetric evaluation of **2d–g** and **3d–f** prototype CIs was done; the obtained results were summarized in Table 2 and are in agreement with those derived from PPC/LPR measurements.

Figure 2 shows a nonlinear relationship between the partition coefficient and the molecular volume versus the efficiencies of **2b–g**, obtained from PPC/LPR at different weight concentrations. It is clear from the graph that the molecules predicted,

such as **2f**, indeed give the best inhibition performance at low doses. It is worth mentioning that the linear relationship between the log *P* and *V*<sub>mol</sub> variables allowed us to construct one graph. The analysis of this graph shows an efficiency-dependent behavior between the increase in concentration and both the log *P* and *V*<sub>mol</sub> variables, implying interesting relationships between efficiency and molecular structure, which is not an artifact of the experimental error bars as stated in some recent studies.<sup>2,4,8</sup>

Figure 3 shows nonlinear relationships between the molar concentration values versus the PPC/LPR measured efficiencies of **2b–g** compounds. Again, the predicted **2f** compound is the best in inhibition performance at low molecular doses. As a matter of fact, the **2e** and **2g** CIs are the best in inhibition

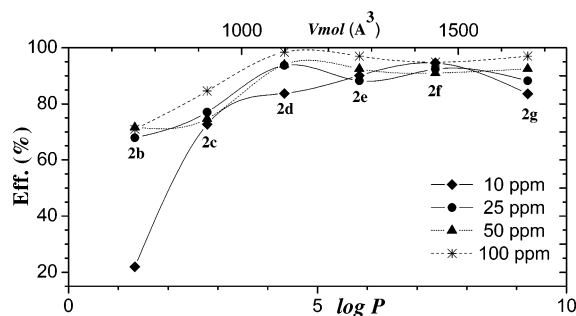


**Figure 2.** Relationship between the partition coefficient,  $\log P$ , and the molecular volume,  $V_{\text{mol}}$ , versus the corrosion inhibition efficiency (PPC/LPR) of compounds **2b–g** in HCl media.

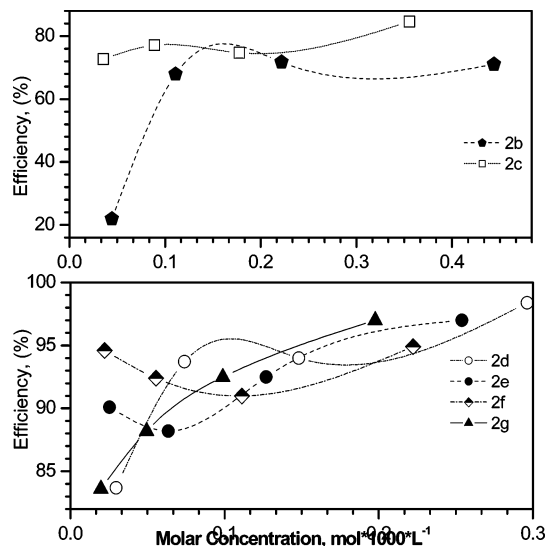


**Figure 3.** Corrosion inhibition efficiency vs molar concentration for **2b–g** CIs.

performance at moderate doses. And finally, at high molar concentration values, the **2d** compound counts on the highest performance for inhibition purposes.

In Figure 3, the presence of curves with double inflection points in **2b** and **2c** is evident. From these curves, the maximum, and hence the best concentration value, is at low dosages, where the minimum is near the critical micellar concentration and shifted to higher doses. In the same figure, compounds **2e** and **2f** present curves with just one inflection point. The minimum in this case coincides with the minimum inhibitory concentration, implying partial removal of the protective film. The isolated case of **2g** is completely parabolic showing increase in inhibition at higher dosages. When a higher molecular concentration is reached in the system, decrease of the efficiencies would tentatively be encountered due to an increase of the free energy of the film formation and, hence, micelle formation processes of the molecules formerly belonging to the protective film. These interesting physicochemical variables will be tentatively understood and confirmed in the next section.

Moreover, the statement that the  $\log P$  and  $V_{\text{mol}}$  are useful variables is herein reinforced since the **2b** and **2c** were the less efficient CIs, with poor indexes as compared against **1** series and observed in Figures 2 and 3, respectively.

### Theoretical Modeling

#### Construction of the Model and Procedure of Simulation.

The semigrand canonical Monte Carlo simulation methodology was applied for the study of a new developed model for CI self-assembled monolayer (SAM) formation under different

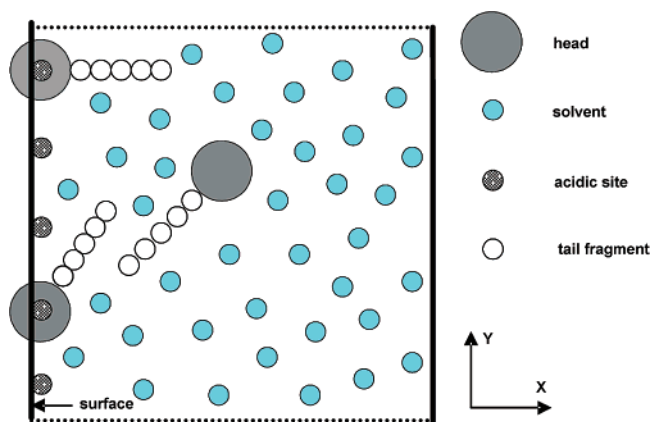


**Figure 4.** Schematic representation of the computational cell. Diameter of the head particles is chosen to be  $\sigma_H = 1.5$ , and the distance between the surface sites is  $r_{ss} = 1.7$ . Thus, the length of the computational cell along the  $Y$  direction is  $L_y = 50r_{ss} = 85$ . The length of the computational cell along the  $X$  direction is chosen large enough to have the homogeneous “bulk” region in the center of the cell:  $30 < L_x < 130$ . The choice of  $L_x$  depends on the considered CI concentration.

conditions. The simulations were performed on a two-dimensional (2D) plane; however, we are confident on qualitative basis that our conclusions will be valid for the three-dimensional counterpart.<sup>42</sup> This simple model was selected for reasons of computational efficiency and to facilitate visual identification of the configurations formed.

Consider a mixture of CI and solvent (W) molecules placed between two hard impenetrable walls separated by a distance  $L_x$ . The inhibitor molecules are modeled as rigid tangentially bonded chains that consist of a head (H) disk and  $m_T$  hard disks of hydrocarbon tail group (T), with diameters  $\sigma_H$  and  $\sigma_T$ , respectively. These molecules are dissolved in a solvent, which is modeled by hard disks of diameter  $\sigma_W$ . The particle–particle pair interaction is given by

$$U_{ii}(r) = \begin{cases} \infty, & \text{if } r < \sigma_i \\ 0, & \text{if } r > \sigma_i \end{cases} \text{ and } U_{ij}(r) = \begin{cases} \infty, & \text{if } r < \sigma_{ij} \text{ } j \neq i \\ 0, & \text{if } r > \sigma_{ij} \end{cases} \quad (1)$$

where the subscripts  $j$  and  $i$  stands for H, T, or W;  $r$  measures the particle separation,  $\sigma_{ij} = 0.5(\sigma_i + \sigma_j)(1 + \Delta_{ij})$ , where  $\Delta_{ij} > 0$  is the nonadditivity parameter.

Within this model corrosion inhibitor, H/T, and solvent media, W, a positive nonadditivity parameter in the cross interaction between the two species,  $\Delta_{ij}$ , favors the homocoordination in comparison to the heterocoordination. As a consequence of the additional repulsion coming from unlike particle interactions, the nonadditivity hard disk mixtures are expected to separate into two phases depending on the parameters of the model, e.g., fluid density, concentration, and nonadditivity.<sup>43–45</sup> In other words, the  $\Delta_{TW}$  parameter takes into account the lyophilicity of CI molecules. A change in  $\Delta_{TW}$  is equivalent to changing the solubility of the CI in the specific solvent. It should be pointed out here that our prototypes of modeled CI molecules are not strictly amphiphilic. However, they interact with each other only through a repulsive potential, and they do associate into micellar configurations.<sup>46</sup> Since in the present work we will consider nonadditivity interaction only between tail chain beads and the solvent,  $\Delta_{TW} \neq 0$ , for the sake of simplicity hereafter, we use the symbol  $\Delta$  instead of  $\Delta_{TW}$ . In all the calculations, it is assumed without loss of generality the diameter of the tail chain bead is chosen to be the unit of length,  $\sigma_T = 1$ . Figure 4 provides an illustration of the geometrical arrangement of CI molecules, solvent, and surface active sites on the left wall.

The above-mentioned H/T/W model mixture is placed inside a sufficiently wide slitlike box with impenetrable walls such that the interaction between particles of each species with box walls is of a hard core type in the  $x$  direction

$$\beta U_{\text{hw}}^a(x) = \begin{cases} \infty, & \text{if } L_X < x, \text{ or } x < 0 \\ 0, & \text{if } L_X > x > 0 \end{cases} \quad (2)$$

where  $x$  is the distance between the center of each fluid particle and the surface in the direction normal to the surface;  $\beta = (kT)^{-1}$ .

The periodic boundary conditions are applied in the  $y$  direction. To mimic the chemisorption of CI molecules, the left wall (at  $x = 0$ ) was considered to have  $N_S$  attractive sites (see Figure 4), to which the H-part of the inhibitor molecules can bond due to the following pair potential

$$\beta U_{\text{as}}^{\text{H}_S}(r_{\text{H}_S}) = \begin{cases} -\epsilon, & \text{if } \lambda_{\text{H}_S} > r_{\text{H}_S} \\ 0, & \text{if } \lambda_{\text{H}_S} < r_{\text{H}_S} \end{cases} \quad (3)$$

Thus, the short-range attraction acts between the surface site and the center of the H-particle and is explicitly given by the narrow square-well potential with a range  $\lambda_{\text{H}_S}$ . The appropriate choice of  $\lambda_{\text{H}_S}$ ,  $\lambda_{\text{H}_S} = 0.2$ , in the present calculations, guarantees that the saturation condition is satisfied; i.e., only one H-particle can be bonded to each surface site.

In addition, the long-range (cut and shifted at  $x_{\text{H}} = 30$ ) Yukawa-type attraction between the left-side wall and the head of the molecules was considered,<sup>22</sup>

$$\beta U_Y(x_{\text{H}}) = K_Y \exp(-0.1x_{\text{H}}) \quad (4)$$

Such potential describes the physisorption process of a CI into the substrate.

Our model mixture is one that does not take into account the real situation, e.g., attractive/repulsive intermolecular interactions. However, we consider that the entropic effect of ordering does play a similar role in an experimental situation as in simulation.

Although our model resembles simple headed molecules, the discussion and conclusions presented herein are not limited to a specific chemical group but can be applied to any surfactant-active species and corrosion inhibitors, e.g., thiols, amines, imidazolines, etc.

The Monte Carlo simulations are performed in the semigrand canonical ensemble,<sup>47</sup> i.e., a constant number of CI particles,  $N_{\text{H}}$ , and average number of solvent particles,  $\langle N_{\text{H}} \rangle$ , at a defined chemical potential  $\beta\mu_{\text{W}} = 1$ . Simulations at constant chemical potential guarantee the same “bulk” density of solvent,  $\rho_{\text{W}} \approx 0.39$ . Our simulations have been performed with  $N_{\text{H}} = 30$  to  $N_{\text{H}} = 210$  CI molecules in the box. The simulations were started by placing the CIs randomly oriented with random positions in the box. The molecules were not permitted to overlap. The system was allowed to evolve, subject to a Metropolis algorithm,<sup>47</sup> until the equilibrium state was reached. The equilibrium state means that the average values of properties described below are unchanged over sequential  $N_{\text{H}} \times 10^8$  MC steps. A MC step consists of the following points: (i) attempts to displace, change of orientation and the head position of one CI molecule, (ii) attempt to move laterally a CI molecule if it is adsorbed on the surface, and (iii) attempts to displace/delete/insert one solvent particle.

The density profiles,  $\rho_i(x)$ , are calculated in MC runs by counting the number of particles,  $N_i$ , in the slabs of thickness,  $\Delta x = 0.05$ , oriented parallel to the  $Y$ -axis using  $\rho_i(x) = \langle N_i \rangle / s_0$ , where  $s_0$  is the slab area,  $s_0 = L_Y \Delta x$ .

**TABLE 3: MC Simulation Results for Adsorption. Number of Occupied Surface Sites<sup>a</sup>**

$m_{\text{T}}$	$\Delta = 0.8$	$\Delta = 0.4$	$\Delta = 0.1$
3	13	12	9
5	15	12	11
6	19	16	10
7	30	22	8
8	13	7	7
9	6	8	6

<sup>a</sup> Number of inhibitor molecules,  $N_{\text{H}} = 70$ , and parameters of attractive potentials are  $\epsilon = -3kT$  and  $K_Y = -4$ .

**TABLE 4: Effect of Solvent Size Ratio,  $\sigma_{\text{W}}/\sigma_{\text{T}}$ , on the Adsorption. MC Simulation Results for Adsorption: Number of Occupied Surface Sites<sup>a</sup>**

$\sigma_{\text{W}}/\sigma_{\text{T}}$	$\Delta = 0.4$	$\Delta = 0.2$	$\Delta = 0.1$
1.2	47	33	27
1	48	35	33
0.8	49	37	26
0.6	46	25	21

<sup>a</sup> Number of CI molecules,  $N_{\text{H}} = 70$ , tail chain length  $m_{\text{H}} = 5$ , and parameters of attractive potentials are  $\epsilon = -3kT$  and  $K_Y = -4$ .

**TABLE 5: MC Simulation Results for Adsorption. Number of Occupied Surface Sites<sup>a</sup>**

$N_{\text{H}}$	$\Delta = 0.8$	$\Delta = 0.4$	$\Delta = 0.2$	$\Delta = 0.1$
30	9	9	7	7
50	11	10	9	8
70	15	12	11	10
140	39	16	15	13
180	32	23	21	15
210	28		25	

<sup>a</sup> Parameters of attractive potentials are  $\epsilon = -3kT$  and  $K_Y = -4$ .

To estimate the inhibition of CI molecules, we have calculated, the averaged value of the substrate surface area,  $\Theta$ , which is the fraction of the sites occupied by the H-part of the CI molecule. In other words, it is assumed that a direct relationship is maintained between the surface covered by the substrate and the inhibition efficiency. Note that, unlike the experiment, the CI concentration in our simulation is defined as a number of CI molecules per length of solid surface,  $X_{\text{H}} = N_{\text{H}} L_Y^{-1}$ , because such definition is more appropriate within our 2D model.

## Simulation Results

A system of CI molecules in the solvent exhibits amphiphilic properties and in consequence triggers a surface adsorption process. Although there is an entropy loss, the free energy of the system reduces due to the orientation of the inhibitor molecules at the interface. CI molecules tend to accommodate themselves preferentially at the solid surface, thereby reducing the interfacial tension. Experimental evidence has suggested that the disposition and stability of a molecular film depend strongly on various experimental parameters and there is a complex interrelationship between the extent of substrate corrosion and the CI SAM thickness, ordering, and chemical structure of the head moiety.<sup>4,48</sup>

Computer simulations were carried out for four CI prototype systems, which were characterized by different nonadditivity parameters:  $\Delta = 0.8, 0.4, 0.2$ , and  $0.1$ . All the conditions and numerical results of simulation are collected in Tables 3–6. As shown below, most of the simulation results were obtained for a CI motif with tail length  $m_{\text{T}} = 5$ . However, we begin discussion with the presentation of the influence of the tail length on the formation of the SAM. As our experimental results show in Figures 2 and 3, the parameter  $m_{\text{T}}$  is an important factor of

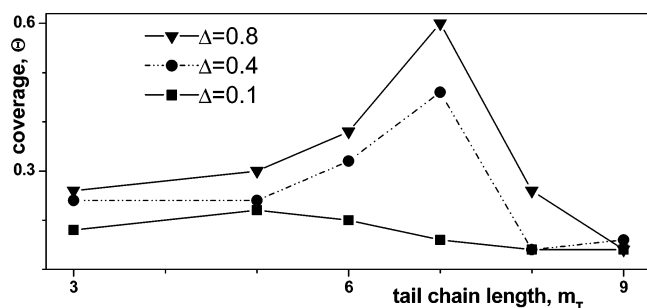


**Figure 5.** Surface coverage,  $\Theta$ , as a function of tail chain length,  $m_T$ , at constant CI concentration,  $X_H = 0.824$  ( $N_H = 70$ ). Three different nonadditives are considered,  $\Delta = 0.8$  (triangles),  $0.4$  (circles), and  $0.1$  (squares). Parameters of attractive potentials are  $\epsilon = -3kT$  and  $K_Y = -4$ .

**TABLE 6: MC Simulation Results for Adsorption: Number of Occupied Surface Sites<sup>a</sup>**

$N_H$	$\Delta = 0.8$	$\Delta = 0.4$	$\Delta = 0.2$	$\Delta = 0.1$
30	12	11	7	6
50	24	14	10	9
70	34	14	10	10
140	37	17	16	14
180	40	17	16	15
210	37	19		

<sup>a</sup> Parameter of attractive potentials is  $\epsilon = -5kT$  and tail chain length is  $m_T = 5$ .

the CI efficiency. This has been pointed out by other research groups too.<sup>14,48,49</sup> Namely, Jennings and co-workers<sup>48,49</sup> found

that SAMs formed from alkanethiols on copper provide improved barrier properties for long chains. This behavior is due to the increased thickness of the barrier film and the improved crystalline character of the thicker films. Their experiments also have implied that SAMs formed from alkyl thiosulfates ( $C_nH_{2n+2}SH$ ) provide corrosion inhibition that was by an order of magnitude higher than for the uncoated metal when  $n = 12$  and  $n = 14$ . Meanwhile,  $C_8H_{18}SH$  and  $C_{10}H_{22}SH$  do not form protective SAMs in water and facilitate corrosion of the copper surface. A similar tendency has been found by Jovanicevic et al.,<sup>14</sup> where the corrosion inhibition of mild steel by imidazolines and their precursors in a carbon dioxide-containing environment was studied. They have stressed that, in contrast to the small effect of the hydrocarbon chain length ( $>C_{12}$ ) on corrosion inhibition reported in the literature,<sup>16</sup> their results established the primary importance of a broad range of molecules ( $C_8$ – $C_{20}$ ) in the corrosion inhibition of imidazolines.

The surface coverage,  $\Theta$ , is presented as a function of tail length,  $m_T$ , in Figure 5. As can be seen, a certain chain length is required in order to form SAMs that provide a high surface coverage and a protective barrier for the underlying surface. The value of  $\Theta$  increases up to a tail length of  $m_T = 7$  (for  $\Delta = 0.8$  and  $0.4$ ) and then sharply decreases. In addition, the present results indicate that the more solvophobic CI molecules (bigger nonadditivity parameter  $\Delta$ ) give higher surface coverage at the same chain length. It is worth noting the similarity in dependence of the CI efficiency on the chain length (molecular volume) to the one discussed above in Figure 2. This is directly related to the density of the adsorbed molecules, e.g., concentra-

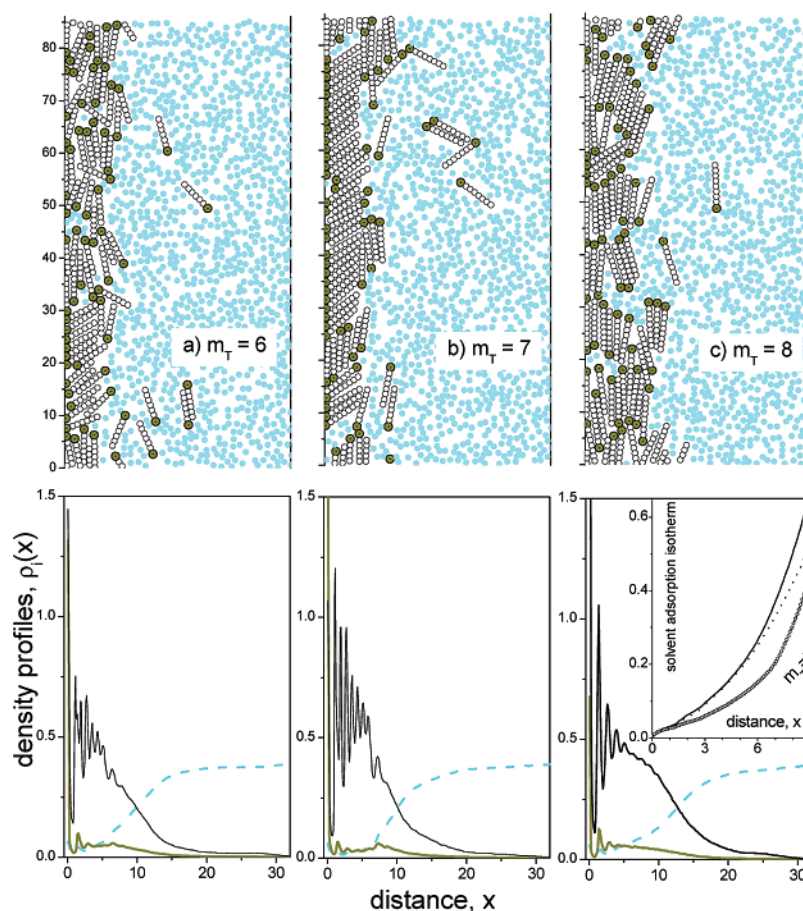


**Figure 6.** Density profiles and snapshots of typical configurations of the model system at three different tail chain lengths,  $m_T = 6, 7$ , and  $8$ , at constant CI molecule concentration,  $X_H = 0.824$  ( $N_B = 70$ ). Parameters of attractive potentials are  $\epsilon = -3kT$  and  $K_Y = -4$ ; nonadditive parameter,  $\Delta = 0.4$ . Black, dark yellow, and cyan dashed lines depict density profiles of tail, head, and solvent particles, respectively. The inset of (c) shows the solvent adsorption isotherm when SAM is formed by CI molecules with  $m_T = 6$  (solid line),  $7$  (circles), and  $8$  (dashed line).



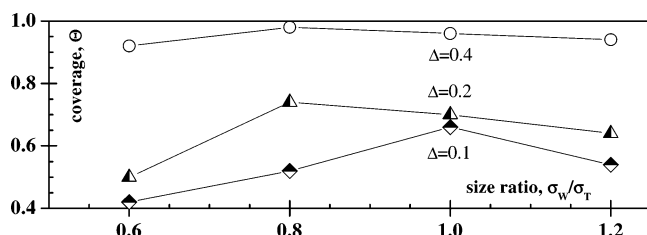


**Figure 7.** Surface coverage,  $\Theta$ , as a function of size ratio,  $\sigma_w/\sigma_T$  at constant CI molecule concentration,  $X_H = 0.824$  ( $N_H = 70$ ). Tail chain length is  $m_T = 5$  and parameters of attraction are  $K_Y = -4$ ,  $\epsilon = -3kT$ . Three different nonadditivities are considered  $\Delta = 0.4$  (circles),  $0.2$  (triangles), and  $0.1$  (diamonds).

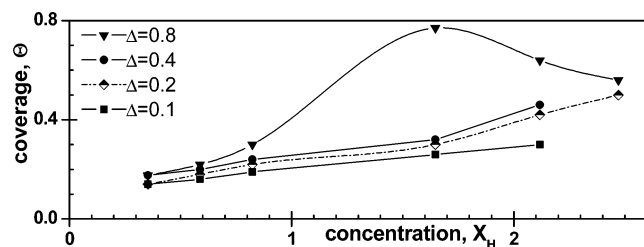


**Figure 8.** Surface coverage,  $\Theta$ , as a function of CI molecule concentration  $X_H$ . Tail chain length is  $m_T = 5$  and parameters of attraction are  $K_Y = -4$ , and  $\epsilon = -3kT$ . Four different nonadditivities are considered,  $\Delta = 0.8$  (triangles),  $0.4$  (circles),  $0.2$  (diamonds), and  $0.1$  (squares).

tion, the number of acidic sites, and solubility, as seen in Figure 3. This means that the molar concentration values are better information trackers when molecular variables are correlated.

To further understand this issue, the local density distribution of the system,  $\rho(x)$ , and the adsorption isotherms of solvent particles on the left wall,  $\Gamma(x)$ , were calculated. We define  $\Gamma(x)$ , as follows,<sup>24</sup>

$$\Gamma(x) = \int_0^x \rho_w(t) dt \quad (5)$$

Some representative results for the local density distributions of the CI and solvent components are plotted in Figure 6, as a function of distance from the left wall at three values of tail chain lengths. The local density is a convenient quantitative characteristics of the self-arrangement of an inhomogeneous fluid in the molecular layer parallel to the substrate surface.<sup>26,44,50</sup>

The sharp and high peaks observed in the immediate vicinity of the substrate reflect a well-localized first layer for CI head and tail chain beads. The inset in Figure 6c presents the adsorption isotherms of solvent particles at three different tail chain lengths,  $m_T = 6, 7$ , and  $8$ . The behavior of  $\Gamma(x)$  shows the lowest value for solvent adsorption and thus the probability of solvent-surface contact when CI SAM is formed by molecules with  $m_T = 7$ .

The reason to form better structured SAMs by CI molecules with  $m_T = 7$  is seen from the upper part of Figure 6, where the simulation plots of typical MC configurations are presented. These graphs as well as the distribution of CI molecular angle of inclination indicate that, at other values of CI tail length, the SAMs are formed by CI molecules that are almost parallel to the surface. Such changes of the self-molecular orientation lead to worse inhibition properties of the CI SAM.

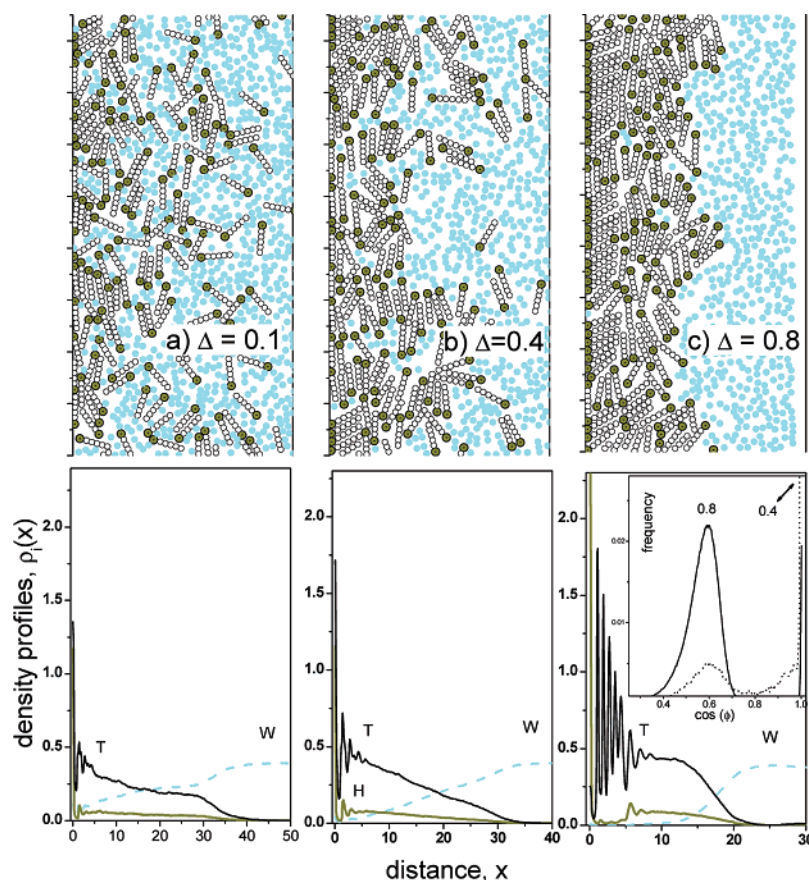


**Figure 9.** Density profiles and snapshots of typical configurations of the model system at three different nonadditive parameters,  $\Delta = 0.1$  (a),  $0.4$  (b), and  $0.8$  (c). Tail chain length is  $m_T = 5$  and CI molecule concentration is  $X_H = 1.65$  ( $N_H = 140$ ). Parameters of attractive potentials are  $\epsilon = -3kT$  and  $K_Y = 4$ . Solid black, solid dark yellow, and cyan dashed lines depict density profiles of tail, head, and solvent particles, respectively. The inset of (c) shows the distribution of inclination, angle  $\Phi$ , of SAM particles for  $\Delta = 0.4$  (dotted line) and  $0.8$  (solid line).

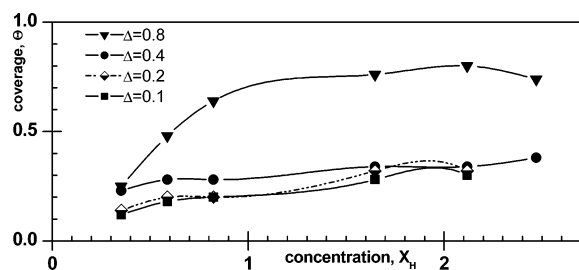


**Figure 10.** Surface coverage,  $\Theta$ , as a function of CI molecule concentration,  $X_H$ . Tail chain length is  $m_H = 5$  and parameters of attraction are  $K_Y = 0$ , and  $\epsilon = -5kT$ . Four different nonaddivities are considered.  $\Delta = 0.8$  (triangles),  $0.4$  (circles),  $0.2$  (diamonds), and  $0.1$  (squares).

In the process of the formation of CI SAMs on a metal surface, the CI molecules assemble and must displace solvent species near or at the surface. They form a densely packed monolayer film. The choice of solvent can affect the properties of the SAM.<sup>51</sup> The solvent molecules with smaller molecular sizes, that interact weaker with the adsorbate, have been shown to produce monolayers with superior properties.

Our simulation results describing the effect of solvent to tail chain bead size ratio,  $\sigma_W\sigma_T^{-1}$ , are presented in Figure 7. At all the nonadditivity values considered, there is a certain size ratio that provides the maximum of surface coverage. When  $\Delta$  increases, the effect of the size ratio almost disappears.

Next, we present the surface coverage at different CI molecule concentrations. First, the combination of chemisorption and physisorption is modeled,  $K_Y = -4$ , and  $\epsilon = -3kT$ . As expected, the increase in concentration,  $X_H$ , promotes a higher surface coverage, Figure 8. However, the CI molecules with

the most solvophobic tails,  $\Delta = 0.8$ , reach a maximum value of  $\Theta$  at  $X_H = 1.65$  (see Table 3) and after that the introduction of the CI leads to a lowering of the surface coverage, i.e., to a SAM with weaker corrosion inhibition properties. As in the cases discussed above, one can observe a higher surface coverage by the SAM formed of CI molecules with more solvophobic tails (bigger nonadditivity parameter  $\Delta$ ). The density profiles and snapshots in Figure 9 illustrate the influence of the  $\Delta$  parameter on the SAM formation. Namely, by comparing the SAMs formed of CI molecules with  $\Delta = 0.4$  and  $0.8$ , one can conclude that the more solvophobic CI provides denser and well-ordered films. The inset of Figure 9c indicates different distributions of the inclination angle of CIs; inhibitor molecules with  $\Delta = 0.4$  are predominantly parallel to the surface, while molecules with  $\Delta = 0.8$  preferentially form an angle of  $\Phi = 54^\circ$  with the surface. Finally, the film formed by the most soluble CI ( $\Delta = 0.1$ ) is the thickest one, however poorly ordered.

In Figure 10, the values of  $\Theta$  are presented as a function of CI concentration,  $X_H$ , without physisorption,  $K_Y = 0$ , and with a strong acidic site-head association,  $\epsilon = -5kT$ . As in the previous case, we observe the same trend of surface coverage at  $\Delta = 0.8$ : increase of CI concentration does not lead to a higher adsorption.

As mentioned in the previous section, our experimental results with **2** type molecules also indicate similar trends. In Figures 2 and 3, one can observe that an increment of the inhibitor concentration is not directly related to better efficiency at the molecular volumes plotted therein. A similar behavior for the inhibition efficiency of a CI molecule, e.g., phosphated ester and ethoxylated nonylphenols in water, has been reported recently by Reyes et al.<sup>52</sup> The variation of CI concentration from

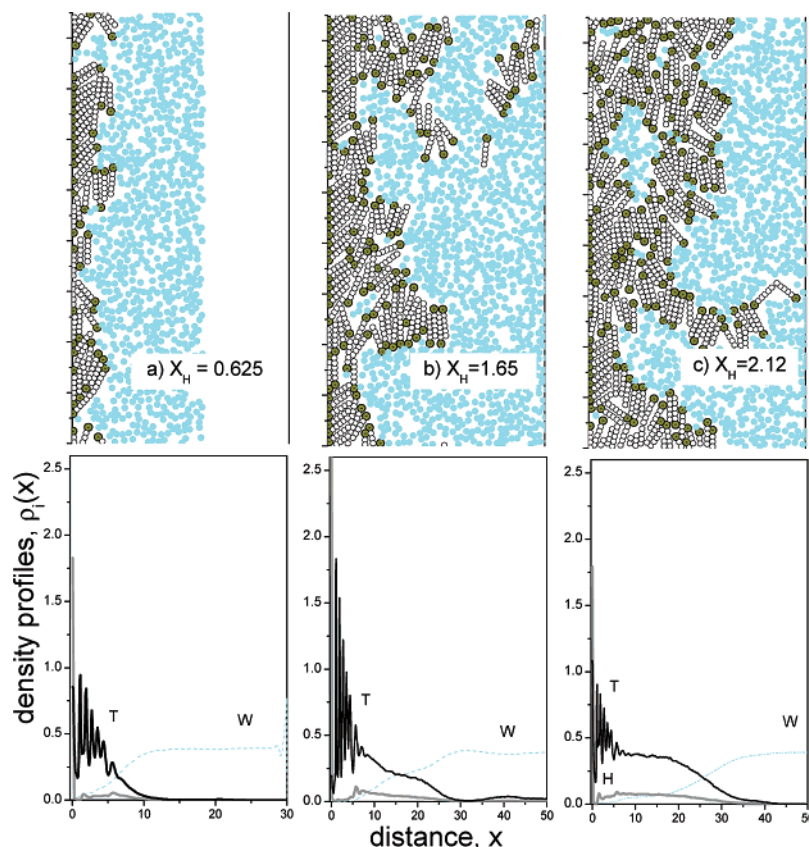


**Figure 11.** Density profiles and snapshots of typical configurations of the model system at three different CI molecule concentrations.  $X_H = 0.625$  (a),  $1.65$  (b), and  $2.12$  (c). Nonadditivity parameter is  $\Delta = 0.8$ , and parameters of attractive potentials are  $\epsilon = -5kT$  and  $K_Y = 0$ . Solid black, solid gray, and cyan dashed lines depict density profiles of tail, head, and solvent particles, respectively.

0.3 to 1.0 g·L<sup>-1</sup> shows that the lowest corrosion rate is obtained at 0.6 g·L<sup>-1</sup>.

To describe the microscopic structure of this system, we have calculated the local density distribution. Some representative results for the local density distributions of CI and solvent components, as a function of distance from the surface, are plotted in Figure 11 for three different concentrations. As can be seen in this figure, an increase in CI concentration yields not a denser film but a thicker one.

Such film thickening is accompanied or induced by the presence of embedded solvent–CI micelles on the surface. The snapshots of the typical configurations, in the upper part of the Figure 11, allow us to conclude that an increase of concentration of the CIs with a certain level of solvophobicity leads to the formation of solloids (surface micelles).<sup>53</sup> Thus, solloids can be considered as an important factor resulting in the decrease of efficiency, when the CI concentration increases. In other words, if the attraction between the CI headgroups and the surface is intermediate in strength, then micelles or solloids will be formed at the surface at higher CI concentrations. This is because the effective attraction between the solvophobic hydrocarbon moieties is stronger than the interaction of the CI headgroups with the surface. The CI adsorption and SAM formation is thus a matter of a balance between the interaction of the CI headgroup with the surface and the *effective* interaction between the hydrophobic moieties of the CI molecules.

Therefore, the “logic” industrial statement to add a little bit more of CI concentration to diminish the corrosion rate causes an inverse effect. This is now tentatively understood using the present simulation findings.

## Conclusions and Perspectives

A strategic algorithm for the design of good CI properties is for the first time developed. Noteworthy is the advance in the theoretical modeling; in this case, the simulations were used as a key designer of new imidazoline-type compounds with enhanced corrosion inhibition properties as well as for understanding of the corrosion inhibition mechanism. The corrosion inhibition efficiency of 1-(2-alkylaminoethyl)-2-alkylimidazolines **2b–g** and their corresponding amides **3b–f** in acid environments is a variable that is directly proportional to the concentration of CI, but with interesting energy fluctuating configurations of the system. The 1-(2-alkylaminoethyl)-2-alkylimidazolines **2b–g** are better corrosion inhibitors than their amidic derivatives **3b–f**; therefore, the inhibition efficiency is highly modulated by the electronic factors present in the molecular structure. For compounds of type 1-(2-alkylaminoethyl)-2-alkylimidazolines, at 25 ppm or lower concentration values, the hydrocarbon tail length and hence the partition coefficient are the main variables that control the inhibition efficiency. Based on the molecular modeling and experimental evidence, it was established that **2b–g** compounds, which possess an iminic nitrogen atom, form stronger coordination bonds with the surface, instead of the weaker bonds present with the amidic precursors.

The MC simulation results confirm the experimental behavior of CIs and tentatively explain the crucial dependence of the corrosion inhibition efficiency on molecular structure (chain length, size ratio between headgroup, and tail chain unit), concentration, and the weak and strong interactions with substrate. While detailed quantitative simulations remain a computational challenge for the future, simple simulations, such as those presented here, may be useful to interpret the experimental data at a qualitative level, which is often the level of the raw industrial data.

**Acknowledgment.** R.G.-R. thanks IMP for a University thesis scholarship. Financial support from Programa de Ingeniería Molecular at the IMP is acknowledged (project D.00178). We are grateful to R. Santillan and O. Pizio for their helpful comments and further manuscript reading.

**Supporting Information Available:** Additional information as noted in text. This material is available free of charge via the Internet at <http://pubs.acs.org>.

## References and Notes

- (1) (a) Zannetti, R. *Chem. Eng.* **1990**, 97, 10. (b) Punckt, C.; Bölscher, M.; Rotermund, H. H.; Mikhailov, A. S.; Organ, L.; Budiansky, N.; Scully, J. R.; Hudson, J. L. *Science* **2004**, 305, 1133. (c) Newman, R. C. *Nature* **2002**, 415, 743. (d) Brown, G. E., Jr. *Science* **2001**, 294, 67.
- (2) Gutzeit, J.; Johnson, J. M. *Corros. Inhibitor Sci. Technol.* **1993**, II-4-1 (NACE).
- (3) Ehmke, E. G. *Mater. Perform.* **1975**, 7, 20.
- (4) Riggs, O. L., Jr. In *Corrosion Inhibitors*; Nathan, C. C., Ed.; NACE: Houston TX, 1979.
- (5) (a) Lyon, S. *Nature* **2004**, 427, 406. (b) Bouayed, M.; Rabaa, H.; Shiri, A.; Saillard, J. Y.; Ben Bachir, A.; Le Beuzed, A. *Corros. Sci.* **1999**, 41, 501.
- (6) (a) Drele, I.; Falewicz, P.; Kuczkowska, S. *Water Res.* **1998**, 32, 3188. (b) Frey, M.; Harris, S. G.; Holmes, J. M.; Nation, D. A.; Parsons, S.; Tasker, P. A.; Winpenny, R. E. P. *Chem. Eur. J.* **2000**, 6, 1407.
- (7) Oppenlaender, K.; Stork, K.; Barthold, K. U.S. Patent 4,388,214, 1983.
- (8) Zamudio, R.; Estrada, A.; Benavides, A.; Benítez J. L. *Rev. Soc. Quím. Mex.* **2002**, 46, 335.
- (9) Flores-Oropeza, E. A.; Lozada-Cassou, M.; Galicia-García, M.; Beltrán, H. I.; George-Tellez, R.; Zamudio-Rivera, L. S.; Morales-Pacheco, A.; Benavides-Lira, A. Mex. Pat. Req. PA/a/2004/012908, 2004.
- (10) Zamudio-Rivera, L. S.; Estrada-Martínez, A.; Morales-Pacheco, A.; Benítez-Aguilar, J. L. R.; Roldan-Perez, R.; Yañez-Ayuso, J. L.; Marin-Cruz, J.; Guzman-Pruneda, M. G. Mex. Pat. Req. PA/a/2002/006434, 2002.
- (11) Zamudio-Rivera, L. S.; Estrada-Martínez, A.; Morales-Pacheco, A.; Benítez-Aguilar, J. L. R.; Rodríguez-Sevilla, A. N.; Guzman-Pruneda, M. G. Mex. Pat. Req. PA/a/2002/002642, 2002.
- (12) Shelton, K.; Bentley, R.; Savage, M. U.S. Patent EP0129506 1992.
- (13) Meyer, G. R. Nalco, Energy Services. WO Patent 2004/092447 A2, 2004.
- (14) Jovancevic, V.; Ramachandran, S.; Price, P. *Corrosion* **1999**, 55, 449.
- (15) Taleb, A.; Chausee, A.; Dymitrowska, M.; Stafiej, J.; Badiali, J. P. *J. Phys. Chem. B* **2004**, 108, 952.
- (16) Ramachandran, S.; Tsai, B. L.; Blanco, M.; Chen, H.; Tang, Y.; Goddard, W. A., III. *Langmuir* **1996**, 12, 6419.
- (17) Ramachandran, S.; Tsai, B. L.; Blanco, M.; Chen, H.; Tang, Y.; Goddard, W. A., III. *J. Phys. Chem. A* **1997**, 101, 83.
- (18) Duda, Y.; Henderson, D.; Pizio, O.; Wasan, D. *Mol. Phys.* **1998**, 94, 341.
- (19) Vakarin, E.; Duda, Y.; Holovko, M. *J. Chem. Phys.* **1997**, 107, 5569.
- (20) Pizio, O.; Henderson, D.; Sokolowski, S. *Mol. Phys.* **1995**, 85, 407.
- (21) Zagorski, R.; Borowko, M.; Sokolowski, S.; Pizio, O. *Mol. Phys.* **1999**, 96, 885.
- (22) Patrykiewicz, A.; Sokolowski, S.; Binder, K. *Surf. Sci. Rep.* **2000**, 37, 207.
- (23) Ruckenstein, E.; Manciu, M. *Langmuir* **2001**, 17, 5464.
- (24) Lee, L. L. *Molecular thermodynamics of nonideal fluids*; Butterworths: Boston, MA, 1988.
- (25) Batina, N.; Huerta, A.; Pizio, O.; Sokolowski, S.; Trokhymchuk, A. *J. Electroanal. Chem.* **1998**, 450, 213.
- (26) Duda, Y.; Trokhymchuk, A.; Sokolowski, S.; Pizio, O. *J. Colloid Interface Sci.* **1997**, 198, 68.
- (27) *General Purpose Electrochemical Software (GPES)* v. 4.4. (Provided with Autolab PGSTAT-3, Eco Chemie B. V., Utrecht, The Netherlands) with PC software control.
- (28) *Corrosion*; ASM Handbook; ASM International: Materials Park, OH, 1987; Vol. 13, p 1232.
- (29) ASTM E 200-97. *Standard Practice for Preparation, Standardization, and Storage of Standard and Reagent Solution for Chemical Analysis*; Muhlstein, C. L., Brown, S. B., Eds.; American Society for Testing and Materials: West Conshohocken, PA, 1997; Sections 34–38.



- (30) ASTM STD G3-89. *Standard Practice for Conventions Applicable to Electrochemical Measurements in Corrosion Testing*; Reapproved, Muhlstein, C. L., Brown, S. B., Eds.; American Society for Testing and Materials: West Conshohocken, PA, 1989, 1999.
- (31) ASTM STD G5-94. *Standard Reference Test Method for Marking Potentiodynamic Anodic Polarization Measurements*; Reapproved, Muhlstein, C. L., Brown, S. B., Eds.; American Society for Testing and Materials: West Conshohocken, PA, 1994, 1999.
- (32) ASTM STD G59-97. *Standard Test Method for Conducting Potentiodynamic Polarization Resistance Measurements*; Muhlstein, C. L., Brown, S. B., Eds.; American Society for Testing and Materials: West Conshohocken, PA, 1997.
- (33) ASTM STD G102-89. *Standard Practice for Calculation of Corrosion Rates and Related Information from Electrochemical Measurements*; Muhlstein, C. L., Brown, S. B., Eds.; American Society for Testing and Materials: West Conshohocken, PA, 1989.
- (34) Mansfeld, F. *Corrosion* **1973**, 29, 397.
- (35) NACE. *Wheel Test Method Used for Evaluation of Film-Persistent Corrosion Inhibitors for Oilfield Applications*; Item 24007, 1995.
- (36) ASTM STD G31-72. *Standard Practice for Laboratory Immersion Corrosion Testing of Metals*; Reapproved, Muhlstein, C. L., Brown, S. B., Eds.; American Society for Testing and Materials: West Conshohocken, PA, 1972, 2004.
- (37) ASTM STD G1-03. *Standard Practice for Preparing, Cleaning, and Evaluating Corrosion Test Specimens*; Reapproved, Muhlstein, C. L., Brown, S. B., Eds.; American Society for Testing and Materials: West Conshohocken, PA, 1967, 2003.
- (38) Semiempirical calculations at the PM3 level of theory were performed with the Hyperchem v.6 program in a P-IV PC at 2.2 GHz. An exhaustive conformational search was applied for all the tested molecules to localize all minima. The stationary points found were classified as minima, at the potential energy surface, through the diagonalization of the Hessian matrix at the same level. The self-consistent field convergence criterion was  $1 \times 10^{-8}$ , and the termination condition rms convergence was  $1 \times 10^{-4} \text{ kcal} \cdot (\text{mol} \cdot \text{\AA})^{-1}$  done with the Polak-Ribiere conjugate-gradient algorithm.
- (39) HyperChem v.6, Hypercube Inc. 115 NW 4th St., Gainesville FL.
- (40) White, C. W.; Webster, S.; Merrett, S.; Harrop, P. *Corros. Sci.* **1993**, 35, 1515.
- (41) Kern, P.; Landolt, D. *Electrochim. Acta* **2001**, 47, 589.
- (42) Urbic, T.; Vachy, V.; Kalyuzhnyi, Y. V.; Southhall, H. T.; Dill, K. A. *J. Chem. Phys.* **2002**, 116, 723.
- (43) Pellicane, G.; Caccamo, C.; Wilson, D. S.; Lee, L. L. *Phys. Rev. E* **2004**, 69, 61202.
- (44) Duda Y.; Vakarin E.; Alejandre J. J. *Colloid Interface Sci.* **2003**, 10, 258.
- (45) Saija, F.; Giaquinta, P. V. *J. Chem. Phys.* **2002**, 117, 5780.
- (46) Abu-Sharkh, B. F.; Hamad, E. Z. *Langmuir* **2004**, 20, 254.
- (47) Smit, B.; Frankel, D. *Understanding of Molecular Simulation*; Academic Press: San Diego, 1996.
- (48) Jennings, G. K.; Laibinis, P. E. *Colloids Surf. A* **1996**, 116, 105.
- (49) Lusk, A. T.; Jennings, G. K. *Langmuir* **2001**, 17, 7830.
- (50) Olivares, W.; Degréve, L.; Villegas, J. C.; Lozada-Cassou, M. *Phys. Rev. E* **2002**, 65, 061702.
- (51) Yan, D.; Saunders, J.; Jennings, G. K. *Langmuir* **2000**, 16, 7562.
- (52) Reyes, Y.; Rodríguez, F. J.; del Río, J. M.; Corea, M.; Vázquez, F. *Prog. Org. Coat.* **2005**, 52, 366.
- (53) Somasundaran, P.; Huang, L. *Adv. Colloid Interface Sci.* **2000**, 88, 179.